Acta Pharmaceutica Sinica B 2021;11(6):1513−1525

Chinese Pharmaceutical Association
Institute of Materia Medica, Chinese Academy of Medical Sciences

Acta Pharmaceutica Sinica B

www.elsevier.com/locate/apsb
www.sciencedirect.com

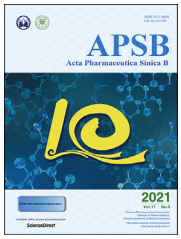

ORIGINAL ARTICLE

Identification of ferroptosis as a novel mechanism for antitumor activity of natural product derivative a2 in gastric cancer

Ying Liu[a], Zan Song[a], Yajie Liu[a], Xubin Ma[a], Wang Wang[a], Yu Ke[a], Yichao Xu[a,*], Dequan Yu[b,*], Hongmin Liu[a,*]

[a]*State Key Laboratory of Esophageal Cancer Prevention & Treatment, Key Laboratory of Advanced Drug Preparation Technologies, Henan Key Laboratory of Drug Quality Control & Evaluation, School of Pharmaceutical Sciences, Zhengzhou University, Ministry of Education of China, Zhengzhou 450001, China*
[b]*State Key Laboratory of Bioactive Substance and Function of Natural Medicines, Institute of Materia Medica, Chinese Academy of Medical Sciences and Peking Union Medical College, Beijing 100050, China*

Received 24 March 2021; received in revised form 25 April 2021; accepted 6 May 2021

KEY WORDS

Jiyuan *Rabdosia rubescens*;
JDA derivative;
Gastric cancer;
Ferroptosis;
ROS;
GPX4;
Ferrous iron;
Autophagy

Abstract Ferroptosis is a type of cell death accompanied by iron-dependent lipid peroxidation, thus stimulating ferroptosis may be a potential strategy for treating gastric cancer, therapeutic agents against which are urgently required. Jiyuan oridonin A (JDA) is a natural compound isolated from Jiyuan *Rabdosia rubescens* with anti-tumor activity, unclear anti-tumor mechanisms and limited water solubility hamper its clinical application. Here, we showed **a2**, a new JDA derivative, inhibited the growth of gastric cancer cells. Subsequently, we discovered for the first time that **a2** induced ferroptosis. Importantly, compound **a2** decreased GPX4 expression and overexpressing GPX4 antagonized the anti-proliferative activity of **a2**. Furthermore, we demonstrated that **a2** caused ferrous iron accumulation through the autophagy pathway, prevention of which rescued **a2** induced ferrous iron elevation and cell growth inhibition. Moreover, **a2** exhibited more potent anti-cancer activity than 5-fluorouracil in gastric cancer cell line-derived xenograft mice models. Patient-derived tumor xenograft models from different patients displayed varied sensitivity to **a2**, and GPX4 downregulation indicated the sensitivity of tumors to **a2**. Finally, **a2** exhibited well pharmacokinetic characteristics. Overall, our data suggest that inducing ferroptosis is the major mechanism mediating anti-tumor activity of **a2**, and **a2** will hopefully serve as a promising compound for gastric cancer treatment.

Abbreviations: 5-FU, 5-fluorouracil; CDX, cell line-derived xenograft; DCFH-DA, dichlorodihydro-fluorescein diacetate; DCM, dichloromethane; IKE, imidazole ketone erastin; JDA, Jiyuan oridonin A; KEGG, Kyoto Encyclopedia of Genes and Genomes; NAC, *N*-acetylcysteine; P_{app}, apparent permeability coefficient; PARP, poly ADP-ribose polymerase; PDX, patient-derived tumor xenograft; PK, pharmacokinetic; qRT-PCR, quantitative real time PCR; ROS, reactive oxygen species; RTV, relative tumor volume; Verp, verapamil.

*Corresponding authors.
E-mail addresses: liuhm@zzu.edu.cn (Hongmin Liu), xuyc2017@zzu.edu.cn (Yichao Xu), dqyu@imm.ac.cn (Dequan Yu).

Peer review under responsibility of Chinese Pharmaceutical Association and Institute of Materia Medica, Chinese Academy of Medical Sciences.

https://doi.org/10.1016/j.apsb.2021.05.006

1. Introduction

Gastric cancer is the fifth most frequent cancer and the third leading cause of death from cancer[1]. Limited therapeutic strategies, especially definite clinical used drugs, prompt the development of new agents against gastric cancer[2]. The Chinese medicinal herb *Rabdosia rubescens* has long been used to treat gastrointestinal tract diseases alone or together with other herbs. Jiyuan oridonin A (JDA) was first isolated and identified by our group, which was named as *ent*-kaurane diterpenoid (I) in the patent applied[3]. However, as in the case with oridonin[4], low aqueous solubility and poor bioavailability significantly limit the clinical application of JDA, impelling scientists to optimize the structure of JDA.

To improve aqueous solubility and bioavailability, a series of JDA derivatives were designed and synthesized. Among them, compound **a2**, bearing a valine ester trifluoroacetate, exhibited excellent anti-proliferative activity against gastric cancer cells. However, the anti-cancer mechanism of **a2** is unclear and needs to be further investigated.

A variety of studies have reported that *ent*-kaurane diterpenes exert anti-tumor effects through regulating cell cycle, apoptosis, autophagy, and metastasis[5–7]. While changes in P53, P21, CDK1/2, CDK2 and cyclin D1 contribute to cell cycle arrest, and the occurrence of apoptosis is associated with disordered expression of BAX, BCL-2, cytochrome *c*, caspase 3/7/9 and PARP. However, these reports mainly focused on the biological effects and the mechanism of action of *ent*-kaurane diterpenes remains unclear. With the development of molecular biology, specific targets of *ent*-kaurane diterpenes have emerged such as NLRP3, AKT, BCR-ABL and peroxiredoxin I[8–11]. Therefore, there is still an urgent need to investigate the mechanism that mediates the anti-cancer activity of **a2**.

Ferroptosis is a form of regulated cell death that is characterized by large amounts of ferrous iron accumulation and lipid peroxidation. SLC7A11 and GPX4 are two key enzymes that repel the lipid reactive oxygen species (ROS) production by transporting L-cystine into cells and reducing lipid peroxides, respectively. Various compounds targeting SLC7A11 or GPX4 show anti-cancer activity[12,13]. Iron is a redox-active metal that is well regulated in cells, elevated levels of iron play a pivotal role in the induction of ferroptosis[14,15]. Thus, induction of ferroptosis is a novel method for the destruction of cancer cells[12,16].

In this research, we show that one JDA derivative **a2** could specifically inhibit the growth of gastric cancer cells. Mechanistically, **a2** induced ferroptosis by decreasing GPX4 and causing ferrous iron accumulation. Furthermore, we found that prevention of ferroptosis strongly rescued the cell growth inhibited by **a2**. Importantly, **a2** differentially prevents tumor growth in gastric cancer patient-derived tumor xenograft (PDX) models, and downregulation of GPX4 can predict the sensitivity of gastric cancer to **a2**, making **a2** a promising therapeutic agent for gastric cancer.

2. Materials and methods

2.1. Reagents

Z-VAD-FMK, 3-methyladenine (3-MA), deferoxamine and RSL3 were obtained from MedChemExpress (NJ, USA); Z-LEHD-FMK and imidazole ketone erastin (IKE) were purchased from Selleck Chemicals (Houston, USA). Dichlorodihydro-fluorescein diacetate (DCFH-DA) was purchased from Beyotime Biotechnology (Shanghai, China). Antibodies against BCL-2, BAX, caspase 9, caspase 3, poly ADP-ribose polymerase (PARP) and β-actin were purchased from Cell Signaling Technology (Boston, MA, USA). Antibodies against SLC7A11 and GPX4 were obtained from Abcam (Cambridge, UK). Antibody against GAPDH was acquired from Goodhere Biological Technology (Hangzhou, China).

2.2. Chemical synthesis

JDA was isolated from extract of Jiyuan *Rabdosia rubescens* as described in patent[17].

General procedure for preparation of JDAO: compound JDA (150 mg, 0.38 mmol) was dissolved in acetone (1 mL). After adding Jones reagent (50 μL), the mixture was stirred for 10 min at 0 °C. The mixture was diluted with water (50 mL) and then extracted with ethyl acetate (50 mL × 3). The extract was then washed with brine, saturated $NaHCO_3$ solution, dried over anhydrous Na_2SO_4, filtered, and evaporated to generate JDAO (135 mg, 91%) without further purification.

General procedure for preparation of **a2**: JDAO (100 mg, 0.14 mmol) was mixed with *N*-Boc-L-valine (0.28 mmol), 1-ethyl-3-(3-dimethylaminopropyl) carbodiimide (29 mg, 0.14 mmol), 4-dimethylaminopyridine (2 mg, 0.016 mmol) and diisopropylethylamine (26 μL, 0.14 mmol) in 3 mL of dichloromethane (DCM). And the reaction was stirred at room temperature for 1−2 h. After completion of the reaction as indicated by TLC, the resulting mixture was poured into DCM (30 mL), and washed with brine (10 mL × 3), and then dried over anhydrous Na_2SO_4 and concentrated under vacuum, and then purified by column chromatography to obtain corresponding product. The corresponding product was de-protected with excessive trifluoroacetic acid (1 mmol) in DCM (6 mL) at 0 °C and stirred for 30 min. After completion of the reaction as indicated by TLC, the reaction solution is concentrated under vacuum. And the residue was purified by crystallization with isopropyl ether to yield compound **a2** as a white solid.

(6*R*,6a*S*,9*S*,11b*S*,14*R*)-14-Hydroxy-4,4-dimethyl-8-methyleneoctahydro-1*H*-6,11b-(epoxymethano)-6a,9-methanocyclohepta[*a*]naphthalene-7,11,12(8*H*,11a*H*)-trione (JDAO), white solid, yield: 95%. m.p.:185.1−185.6 °C. IR (KBr, cm^{-1}): 3565, 2960, 1760, 1733, 1644, 1380, 1105, 1042, 946, 718. ^{1}H NMR (400 MHz, DMSO) δ 6.14 (s, 1H), 6.06 (s, 1H), 5.79 (s, 1H), 4.79−4.78 (m, 1H), 3.73 (s, 1H), 3.11−3.09 (d, J = 8.4 Hz, 1H), 2.96 (s, 1H), 2.91−2.84 (m, 2H), 2.70−2.63 (m, 1H), 2.55 (m, 1H), 1.80−1.73 (m, 1H), 1.62−1.56 (m, 2H), 1.37−1.34 (d,

J = 11.2 Hz, 2H), 1.11−0.94 (m, 2H), 0.81 (s, 3H), 0.72 (s, 3H). ^{13}C NMR (101 MHz, DMSO) δ 204.70, 200.62, 174.52, 148.36, 121.48, 73.07, 70.74, 58.73, 57.93, 46.71, 45.56, 43.18, 41.28, 40.09, 33.99, 30.75, 28.47, 23.55, 19.29, 18.40. HR-MS (ESI): *m/z* Calcd. for $C_{20}H_{25}O_5$ $[M+H]^+$: 345.1702, found 345.1690.

(6*R*,6a*R*,9*S*,11b*S*,14*R*)-4,4-Dimethyl-8-methylene-7,11,12-trioxododecahydro-1*H*-6,11b-(epoxymethano)-6a,9-methanocyclohepta[*a*]naphthalen-14-yl valinate (**a2**), white solid, yield 81%, m.p.:183.1−183.9 °C. IR (KBr, cm^{-1}): 3125, 2969, 1738, 1678, 1532, 1400, 1202, 1137, 1038, 722. ^{1}H NMR (400 MHz, DMSO) δ 8.48 (s, 2H), 6.26 (s, 1H), 5.94 (m, 1H), 4.90−4.85 (m, 2H), 4.04 (m, 1H), 3.41−3.39 (dd, J = 12.0, 4.0 Hz, 1H), 3.30 (d, J = 8.1 Hz, 1H), 2.87−2.85 (m, 2H), 2.81−2.79(dd, J = 13.7, 8.5 Hz, 1H), 2.79−2.67 (m, 1H), 2.05−2.04 (m, 1H), 1.80−1.79 (m, 1H), 1.77−1.68 (m, 2H), 1.40−1.37 (m, 2H), 1.10−1.03 (m, 2H), 0.89 (s, 3H), 0.87 (s, 3H), 0.82 (s, 3H), 0.72 (s, 3H). ^{13}C NMR (101 MHz, DMSO) δ 203.14, 198.01, 173.90, 167.92, 158.31, 158.00, 145.94, 123.17, 75.08, 72.16, 58.85, 56.19, 46.39, 45.27, 43.16, 38.46, 33.81, 30.48, 29.34, 28.11, 22.97, 18.92, 18.18, 18.12, 17.11. HR-MS (ESI): *m/z* Calcd. for $C_{25}H_{34}NO_6$ $[M+H]^+$: 444.2386, found 444.2381.

2.3. Cell lines and proliferation assay

Human gastric cancer cell lines HGC-27, MGC-803, BGC-823 and AGS, and human immortalized gastric mucosa epithelial cell line GES1 were purchased from Chinese Academy of Science Cell Bank (Shanghai, China). Gastric cancer cell lines SGC-7901 and MKN-45 were kindly provided by Ding Jian (Shanghai Institute of Materia Medica, Chinese Academy of Sciences, Shanghai, China). Cell proliferation was measured by sulforhodamine B (SRB; Sigma−Aldrich, St. Louis, MO, USA) assay as described previously[18].

$$\text{Relative cell growth} = (OD_{treated} - OD_{start}) / (OD_{control} - OD_{start}) \quad (1)$$

$$\text{Relative inhibitory rate (\%)} = (OD_{control} - OD_{treated}) / (OD_{control} - OD_{start}) \times 100 \quad (2)$$

OD_{start} means the optic density of cells at the moment of adding test compounds.

2.4. Measurement of cell cycle, cell apoptosis, mitochondrial membrane potential and intracellular ROS

Measurement of cell cycle, cell apoptosis, mitochondrial membrane potential and intracellular ROS have been described previously[18].

2.5. RNA-seq analysis

MGC-803 cells seeded in 6-well plates were treated with **a2** (10 μmol/L) for 24 h. Total RNA of cells were then extracted by TRIzol reagent (Solarbio Science & Technology Co., Beijing, China). cDNA library preparation, RNA sequencing, quality control and transcriptome profiling were performed by Novogene (Beijing, China). Briefly, total RNA were verified by agarose gel electrophoresis, Nanodrop, and Agilent 2100 analysis, following by cDNA library preparation with poly (A) selection and RNA sequencing with Illumina PE150. Raw data of RNA sequencing were aligned by Hisat2 and quantified by HTSeq, producing the data of sample read counts and FPKM. RNA-seq data was further analyzed by R packages DESeq2 and clusterProfiler to generate differentially expressed mRNAs and enriched pathways[19,20].

2.6. Measurement of lipid peroxidation using C11-BODIPY$^{581/591}$

Cells seeded in 6-well plates were treated with **a2** for 6 h, cells were then collected and re-suspended in 500 μL PBS containing 2 μmol/L C11-BODIPY$^{581/591}$ (Thermo Fisher Scientific, MA, USA) for 30 min at 37 °C. Subsequently, cells were measured by BD LSRFortessa flow cytometry (NJ, USA). Quantification of data was performed with Flowjo.

2.7. Quantitative real time PCR (qRT-PCR)

Total RNAs were extracted from cultured cells using the TRIzol reagent. cDNAs were generated by reverse transcription using HiScriptII Q RT SuperMix (Vazyme, Nanjing, China). qRT-PCR was performed with ChamQ Universal SYBR qPCR Master Mix (Vazyme) against specific genes. Relative quantity of gene expression was normalized to GAPDH and analyzed by QuantStudio™6 Flex Real-Time PCR System (Thermo Fisher Scientific). The gene-specific primer pairs, which were synthesized by GENEWIZ (Jiangsu, China), were as follows, respectively: GAPDH-F, 5′-GCACCGTCAAGGCTGAGAAC-3′; GAPDH-R, 5′-TGGTGAAGACGCCAGTGGA-3′; GPX4-F, 5′-GAGGCAAGACCGAAGTAAACTAC-3′; GPX4-R, 5′-CCGAACTGGTTACACGGGAA-3′; SLC7A11-F, 5′-GGTCCATTACCAGCTTTTG TACG-3′; SLC7A11-R, 5′-AATGTAGCGTCCAAATGCCAG-3′.

2.8. Transfection and generation of stable cell lines

Plasmid GPX4 (GV641) and lentivirus particles were generated by GeneChem Co. (Shanghai, China). Gastric cancer cells were seeded in 6-well plates and infected with viruses according to manufacturer's instruction, multiplicity of infection for MGC-803 and MKN-45 was 10 and 25, respectively. After 72 h, stably transfected cells were selected and maintained with puromycin (2.5 μg/mL).

2.9. RNA interference

Gastric cancer cells were seeded in 12-well plate, cells were then transfected with specific siRNAs using GP-transfect-Mate (GenePharma Co., Shanghai, China) according to manufacturer's protocols. After 12 h, cells were digested with trypsin and seeded in 96-well plate to test the anti-proliferative activity of compound **a2**. The targeted genes sense sequences were as follows, siSLC7A11#1: 5′- GCAGCUACUGCUGUGAUAUTT-3′, siSLC 7A11#2: 5′-CCAUGAUUCAUGUCCGCAATT-3′. The negative control was provided by GenePharma Co.

2.10. Intracellular ferrous iron (Fe^{2+}) determination

Cells seeded in 60-mm plates were treated with compounds for indicated time, cells were then collected and homogenized in iron assay buffer. Intracellular ferrous iron content was determined using the iron assay kit from Sigma−Aldrich (MAK025) according to instructions provided by manufacturer.

2.11. Gastric cancer cell line-derived xenograft (CDX) studies

All animal experiments were performed in accordance with relevant protocols and guidelines approved by animal care and committee of Zhengzhou University (Zhengzhou, China). Male nude mice (ages 6−8 weeks) used in the studies were purchased from Hunan SJA Laboratory Animal Co. (Changsha, China). Male nude mice were subcutaneously injected with MGC-803 cells into the right flank of mouse. Once the tumor volume reached 100−200 mm^3, mice were randomly divided into 5 groups (6 mice/group) and administered with saline, **a2** (5, 10, and 20 mg/kg), or 5-fluorouracil (5-FU, 15 mg/kg) once a day for 21 days *via* tail vein injection. Tumor volume (tumor length × $width^2$/2) and body weight were recorded every two days. All mice were sacrificed after the final treatment, tumors were isolated and weighed, and liver, kidney, lung, heart, and spleen were collected to perform histopathological examination.

2.12. Gastric cancer PDX studies

Fresh surgical tumor specimens of patients bearing gastric cancer were collected from the First Affiliated Hospital of Zhengzhou University. Before the tissue collection, the clinical protocol was approved by the ethics review board of the First Affiliated Hospital of Zhengzhou University. After examination by pathologists, tumor tissues resected from primary lesion were transferred to storage solution (RPMI 1640 medium supplemented with 2% FBS, and 5% amphotericin B). Tumors were dissected into 1 mm^3 and subcutaneously implanted into NOD-SCID mice within 6 h. After tumor tissues were stably propagated for three passages, tumor tissues were used for evaluating the anti-tumor activity of **a2** with the similar method described in gastric cancer CDX studies. Treatment duration of PDX mice varied from 15 to 36 days according to tumor volumes in control groups. The relative tumor volume (RTV) was determined according to Eq. (3):

$$\mathrm{RTV} = V_x/V_0 \quad (3)$$

V_x represented the tumor volume on Day x and V_0 represented tumor volume on Day 0. The "treated/control" (T/C) ratio was determined according to Eq. (4):

$$\mathrm{T/C}\ (\%) = \mathrm{RTV_T/RTV_C} \times 100 \quad (4)$$

RTV_T and RTV_C represented the RTV of treated and control group, respectively.

2.13. Pharmacokinetic studies

Pharmacokinetic studies including Caco-2 permeability assay ($n = 2$), metabolic stability in liver microsomes ($n = 2$) and pharmacokinetic parameters in rats ($n = 3$) were conducted by Sundia MediTech Company (Shanghai, China).

2.14. Statistical analysis

The data are the means of at least three independent experiments and presented as mean ± standard deviation (SD). Statistical differences were assessed by one-way or two-way ANOVA analysis with GraphPad Software according to experiments. $P < 0.05$ was considered statistically significant. $P < 0.05$, $^*P < 0.01$, $^{**}P$ 0.005, $^{***}P$ 0.001.

3. Results

3.1. Compound *a2* markedly inhibited the growth of gastric cancer cells

Inspired by the modification of oridonin with amino acid[21], our group designed and synthesized a series of JDA derivatives (data not published) and **a2** was selected for further investigation (Fig. 1A). To test the anti-proliferative effect of **a2** in gastric cancer cells, the GI_{50} values of **a2** were determined in the human gastric epithelial cell line GES1 and six gastric cancer cell lines MGC-803, HGC-27, SGC-7901, MKN-45, AGS and BGC-823. As shown in Fig. 1B, the GI_{50} values of **a2** against gastric cancer cells ranged from 0.88 to 3.33 μmol/L, whereas the GI_{50} values of **a2** in GES1 were at least five-fold higher than those in gastric cancer cells, suggesting that the **a2** selectively inhibited the growth of gastric cancer cells. Next, MGC-803 and SGC-7901 cells were selected to make further investigation. We found **a2** decreased the number of MGC-803 cells in time- and dose-dependent manner, and **a2** induced morphologic changes of cells as early as 1 h after incubation at high concentrations (5 and 10 μmol/L, Fig. 1C and D). In addition, the relative cell growth of cells was gradually decreased after **a2** treatment at 10 μmol/L compared with that of other cell groups, indicating that **a2** led to cell death at high concentrations. Similar results were observed in MKN-45 cells (Supporting Information Fig. S1A and S1B).

Given that **a2** markedly suppressed cell growth, we tried to determine whether the cell cycle was affected by **a2**. The results showed that **a2** significantly increased the cell population in the G2/M phase and reduced the number of cells in the S phase (Fig. 1E). Similar phenomenon was obtained in MKN-45 cells (Fig. S1C and S1D). Therefore, **a2** showed significant anti-proliferative activity against gastric cancer cells and arrested them in the G2/M phase.

3.2. Compound *a2* induced mitochondria-dependent apoptosis in gastric cancer cells

Considering that **a2** caused cell death at high concentrations and that variety of *ent*-kaurane diterpenoids induce cell apoptosis, we examined whether **a2** can induce cell apoptosis. As shown in Fig. 2A−D, **a2** significantly elevated cell populations co-staining with PI and Annexin V-FITC in dose- and time-dependent manner, indicating that **a2** induced apoptosis. Apoptosis induced by **a2** was also observed in MKN-45 cells (Supporting Information Fig. S2A−S2D). Mitochondrial membrane potential was measured by JC-1 staining, loss of which marks the initiation of mitochondria-dependent apoptosis[22]. Compound **a2** markedly induced the loss of mitochondrial potential, indicating that **a2** caused mitochondrial injury (Fig. 2E and F, Fig. S2E and S2F). Apoptosis-related proteins were further examined. As shown in Fig. 2G and Fig. S2G, **a2** dose-dependently decreased the levels of anti-apoptotic protein BCL-2 and elevated cleaved-caspase 9/3 and PARP proteins, confirming that **a2** induced mitochondria-dependent apoptosis in gastric cancer cells.

To explore the contribution of apoptosis to the anti-tumor activity of **a2**, the pan-caspase inhibitor Z-VAD-FMK or selective caspase 9 inhibitor Z-LEHD-FMK were utilized to investigate the role of apoptosis. In MGC-803 cells, the presence of Z-VAD-FMK and Z-LEHD-FMK partially antagonized anti-proliferative activity of **a2** (Fig. 2H). However, combination of **a2** with Z-VAD-FMK or Z-LEHD-FMK caused equivalent relative inhibitory rate

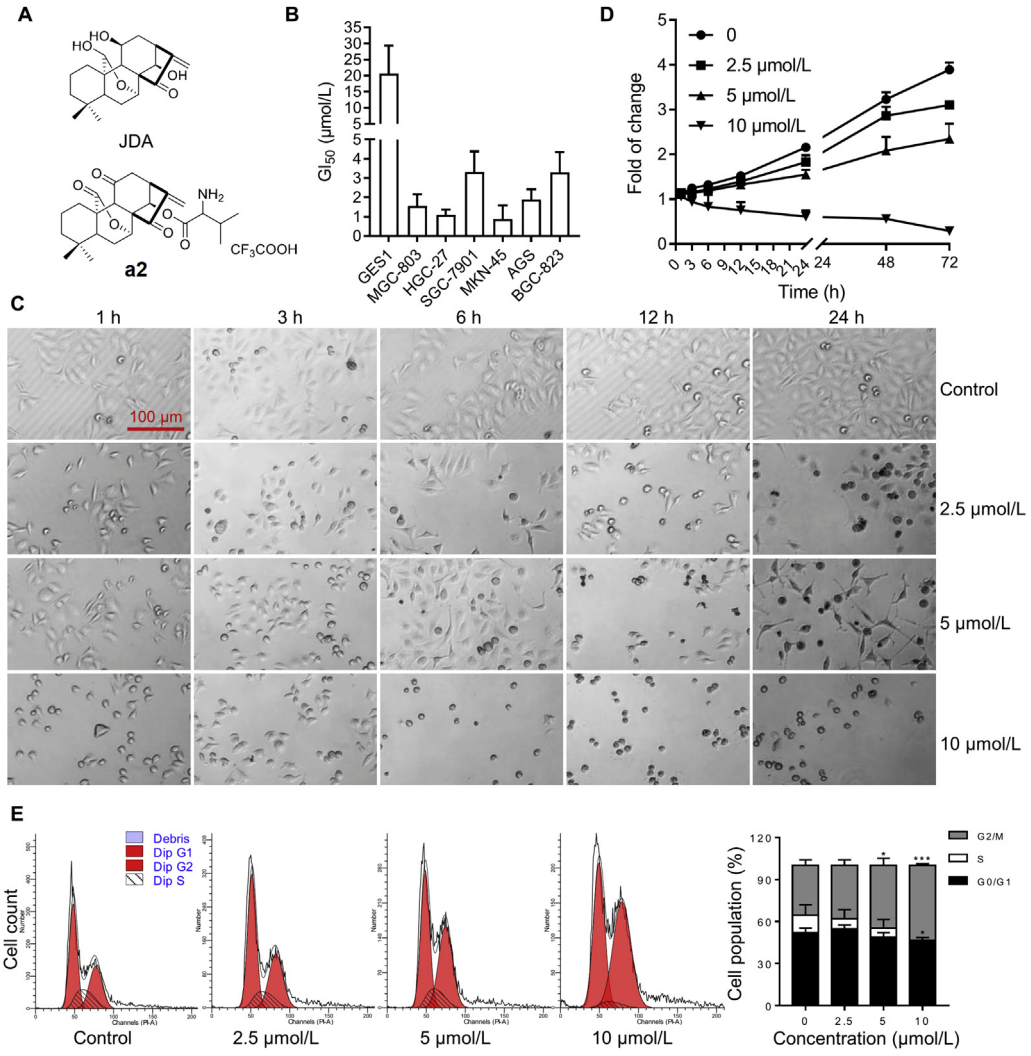

Figure 1 Compound **a2** selectively inhibited the growth of gastric cancer cells. (A) Structural formulas of JDA and **a2**. (B) GI_{50} values of **a2** in selected cells for 72 h. (C) MGC-803 cells were treated with **a2** at indicated doses and then were imaged by the bright-field microscopy at specific point in time. (D) MGC-803 cells were treated with **a2** at indicated concentrations for different time duration and then cell viability was detected by SRB staining. (E) MGC-803 cells were treated with **a2** for 48 h, cells were then stained with PI and analyzed by flow cytometry and quantified. Data are presented as the mean ± SD ($n = 3$) from three independent experiments with biological duplicates in (B, D, E). Statistics differences were analyzed by two-way ANOVA analysis (E): $^{*}P < 0.05$, $^{***}P < 0.005$ *vs*. the control.

with that of **a2** alone in MKN-45 cells, suggesting that **a2** inhibited cell growth independent of apoptosis (Fig. S2H). Thus, **a2** can induce apoptosis in both MGC-803 and MKN-45 cells, whereas cell growth inhibited by **a2** partially relied on apoptosis only in MGC-803 cells.

*3.3. Identification of ferroptosis induced by compound **a2** in gastric cancer cells*

To further explore the mechanism mediating the anti-cancer effect of **a2**, mRNAs extracted from control and treated MGC-803 cells were analyzed for differentially expressed genes. As shown in Fig. 3A, there were 560 significant differentially expressed mRNAs affected by **a2** in MGC-803 cells (Supporting Information Table S1). Kyoto Encyclopedia of Genes and Genomes (KEGG) enrichment analysis of these 560 mRNAs showed that the genes were mainly enriched in proteasome, antigen processing and presentation, ferroptosis, phagosome, etc (Fig. 3B). Given that ferroptosis is a type of programmed cell death initiated by large amounts of ROS and most of *ent*-kaurane diterpenes caused ROS elevation in cancer cells, we further presented the ferroptosis-related mRNAs affected by **a2**. Compound **a2** affected mRNAs encoding ferroptosis-related proteins in a seemingly paradoxical manner: the mRNA encoding key anti-ferroptosis kinase GPX4 was decreased, whereas **a2** elevated the mRNA encoding the anti-ferroptosis protein SLC7A11 (Fig. 3C). To explore whether **a2** induces ferroptosis, lipid ROS were determined with C11-BODIPY$^{581/591}$. Compound **a2** dose-dependently elevated lipid ROS production in both MGC-803 and MKN-45 cells, confirming that **a2** induced cell ferroptosis (Fig. 3D and Supporting Information Fig. S3A). In addition, total ROS were measured, elevation of which will initiate ferroptosis. Compound **a2** markedly elevated the level of ROS, and ROS scavenger *N*-acetylcysteine (NAC) almost totally reversed ROS accumulation triggered by **a2** (Fig. 3E and Fig. S3B). In accordance with that of ROS change, NAC can dramatically rescue cell growth prevented by **a2** (Fig. 3F and Fig. S3C). Furthermore, transmission electron

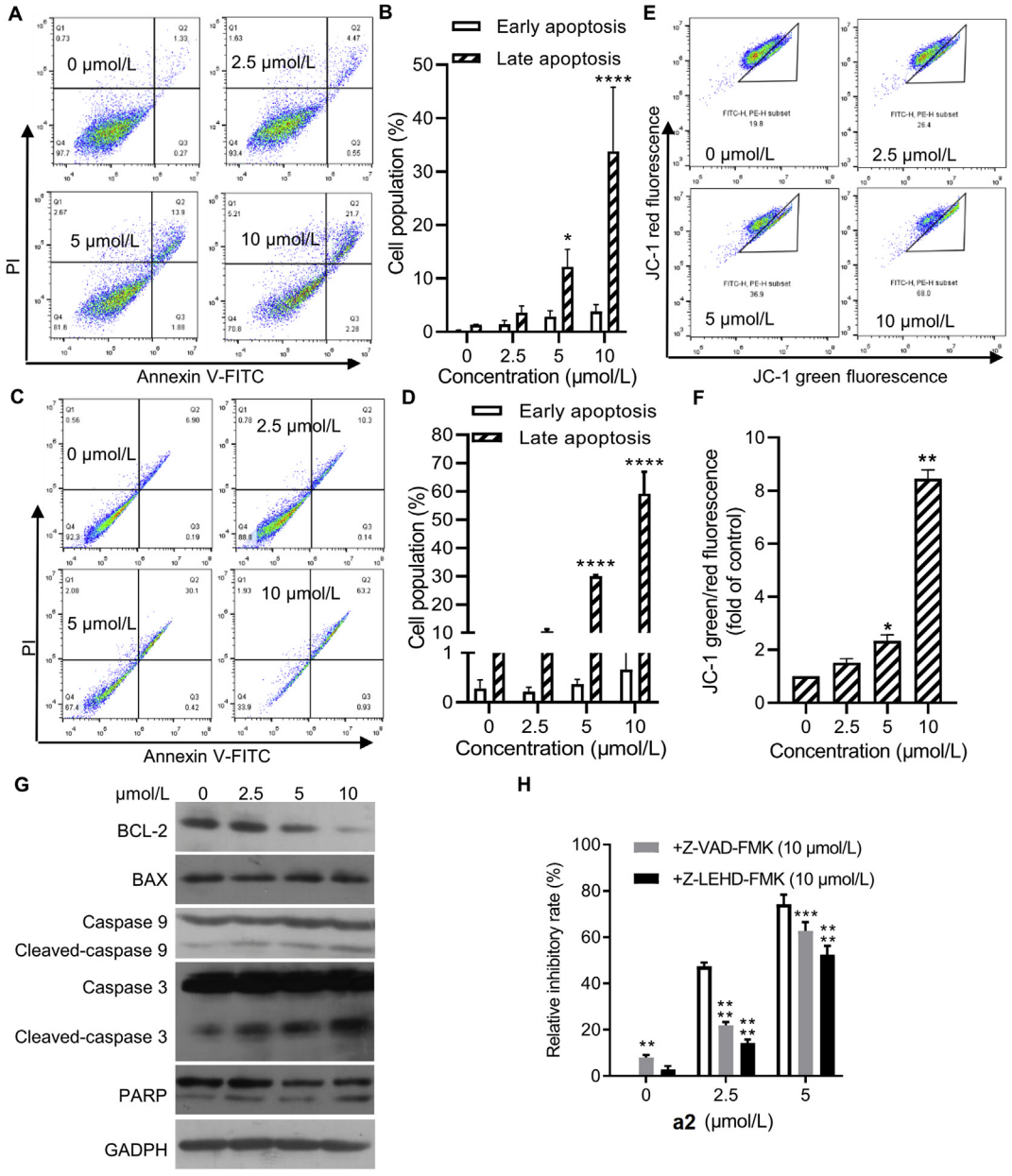

Figure 2 Compound **a2** induced mitochondria-dependent apoptosis in gastric cancer cells. MGC-803 cells were treated with **a2** at indicated concentrations for 24 h (A and B) and 48 h (C and D), cells were then stained by PI and Annexin V-FITC and analyzed by flow cytometry. (E and F) MGC-803 cells were treated with **a2** for 24 h, cells were then stained by JC-1 and analyzed by flow cytometry. (G) MGC-803 cells were treated with **a2** for 24 h with illustrated concentrations, indicated proteins were tested by Western blot. (H) MGC-803 cells were treated with **a2** alone or in combination with the indicated agents for 72 h, cell viability was then tested by SRB assay. Data are presented as the mean ± SD ($n = 3$) from three independent experiments with biological duplicates in (B, D, F, H). Statistics differences were analyzed by two-way ANOVA analysis (B, D, H) or one-way ANOVA analysis (F): $^{*}P < 0.05$, $^{**}P < 0.01$, $^{****}P < 0.001$ *vs*. the control (B, D, F). $^{**}P < 0.01$, $^{***}P < 0.005$, $^{****}P < 0.001$ *vs*. the **a2** treated samples (H).

microscopy examination showed that mitochondria became smaller and with increased membrane density in **a2**-treated cells compared with those in control cells (Fig. 3G). Thus, **a2** can induce ferroptosis in gastric cancer cells.

3.4. *Compound **a2** induced ferroptosis via decreasing GPX4*

SLC7A11 and GPX4 are two important proteins that negatively regulate ferroptosis by importing L-cystine and catalyzing the reduction of lipid peroxides, respectively[23]. However, **a2** induced the opposite alteration of SLC7A11 and GPX4 in MGC-803 cells (Fig. 3C). qRT-PCR analysis confirmed that **a2** dose-dependently reduced the mRNA level of GPX4 and increased the mRNA level of SLC7A11 in both MGC-803 and MKN-45 cells (Fig. 4A and B). The protein levels of GPX4 and SLC7A11 affected by **a2** were consistent with that of the changes in mRNAs (Fig. 4C). To investigate the biological function of GPX4 in **a2**-induced cell arrest, GPX4 was

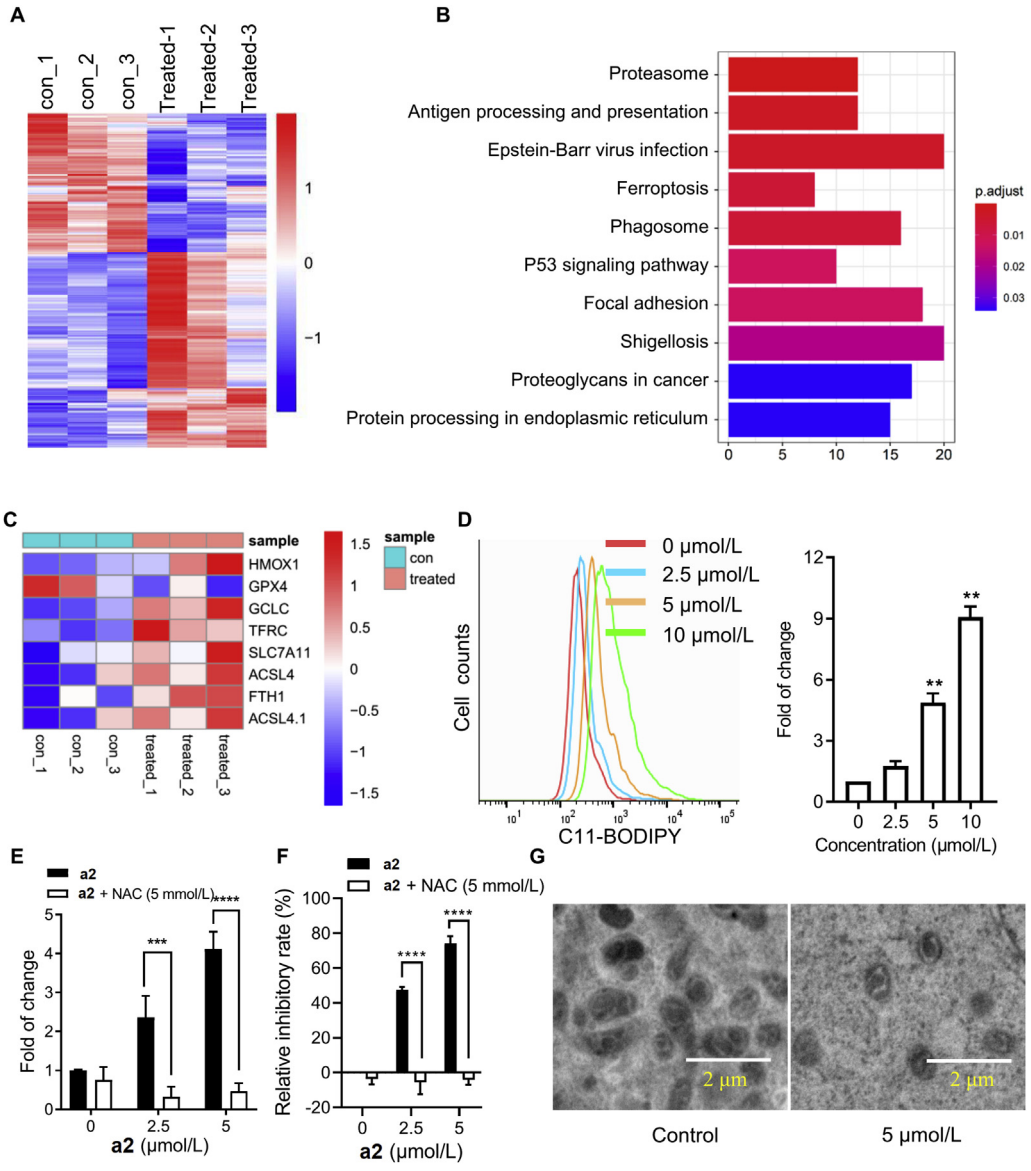

Figure 3 Identification of ferroptosis induced by compound **a2** in gastric cancer cells. (A) Heatmap of differentially expressed mRNAs after incubation of MGC-803 cells with **a2** (10 μmol/L) for 24 h (RNA-seq, $n = 3$), $P < 0.05$, basemean of read > 100. (B) KEGG pathways of differentially expressed mRNAs in **a2** treated *vs*. control MGC-803 cells. Bar color represents statistical significance of the enrichment, length of bar indicates gene number. (C) Heatmap of differentially expressed mRNAs in ferroptosis pathway in **a2** treated *versus* control MGC-803 cells. (D) MGC-803 cells were treated with **a2** for 6 h, cells were then stained by C11-BODIPY$^{581/591}$ and analyzed by flow cytometry. (E) MGC-803 cells were treated with **a2** in the absence or presence of NAC for 24 h, cells were then stained with DCFH-DA and analyzed by flow cytometry. (F) MGC-803 cells were treated with **a2** in the absent or present of NAC for 72 h, relative inhibitory rates of compounds were determined with SRB assay. (G) MGC-803 cells were treated with **a2** for 6 h, cells were then observed by transmission electron microscopy. Data are presented as the mean ± SD ($n = 3$) from three independent experiments with biological duplicates in (D and F). Statistics differences were analyzed by one-way ANOVA analysis (D) or two-way ANOVA analysis (E and F): $^{**}P < 0.01$ *vs*. the control (D). $^{***}P < 0.005$, $^{****}P < 0.001$ *vs*. the **a2** treated samples (E and F).

overexpressed in gastric cancer cells. GPX4 overexpression significantly reversed the cell growth inhibited by **a2** in both MGC-803 and MKN-45 cells (Fig. 4D and E). Next, we found GPX4 inhibitor RSL3 and **a2** exerted additive anti-proliferative activity against MGC-803 cells at the low concentration (Supporting Information Fig. S4B), indicating that both RSL3 and **a2** exerted anti-cancer activity through inhibiting GPX4. In addition, we measured the expression level of GPX4 in a panel of cell lines. Concerning GI_{50} value of **a2** in different cell lines, we found that the cell lines with high expressed GPX4 were more sensitive to **a2** (Fig. S4A and Fig. 1B).

We then tested the biological function of SLC7A11 in anti-tumor activity of **a2** with the specific system x_c^- inhibitor IKE. IKE alone had no effect on cell growth, whereas the combination of IKE and **a2** significantly augmented the relative inhibitory rate induced by **a2** alone in both MGC-803 and MKN-45 cells, indicating that elevated SLC7A11 antagonized **a2**-induced cell growth inhibition (Fig. 4F and G). In addition, **a2** showed higher relative

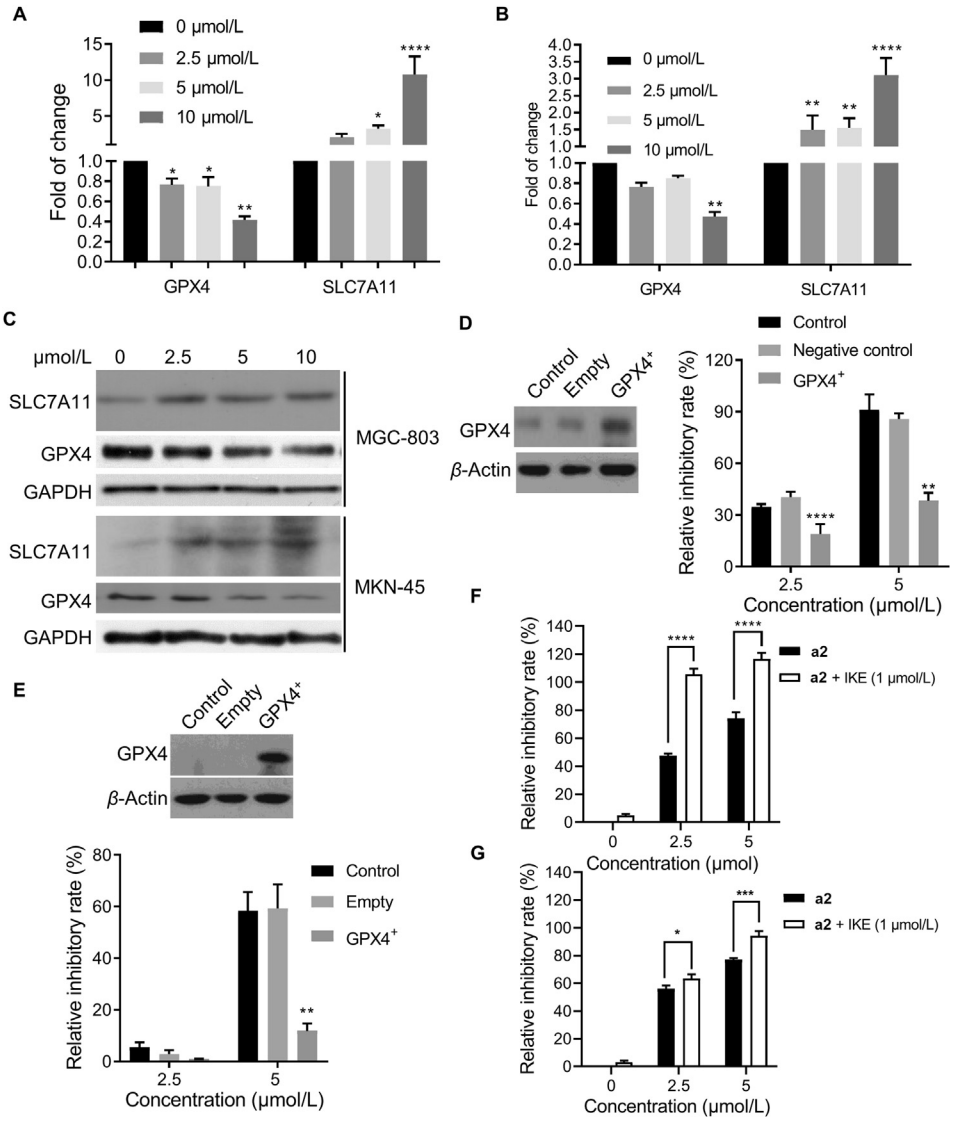

Figure 4 Compound **a2** induced ferroptosis *via* decreasing GPX4. MGC-803 (A) and MKN-45 (B) cells were treated with **a2** at indicated doses for 24 h, indicated mRNAs were then determined by qRT-PCR. (C) MGC-803 and MKN-45 cells were treated with **a2** for 24 h, indicated proteins were measured. GPX4 were overexpressed in MGC-803 (D) and MKN-45 (E) cells, relative inhibitory rates of **a2** in indicated cells for 24 h were tested. MGC-803 (F) and MKN-45 (G) cells were treated with **a2** alone or combined with IKE for 72 h, cells were then examined by SRB assay. Data are presented as the mean ± SD ($n = 3$) from three independent experiments with biological duplicates in (A−B, D−G). Statistics differences were analyzed by one-way ANOVA analysis (A and B) or two-way ANOVA analysis (D−G): $^{*}P < 0.05$, $^{**}P < 0.01$, $^{****}P < 0.001$ *vs*. the control (A−B, D−E). $^{*}P < 0.05$, $^{***}P < 0.005$, $^{****}P < 0.001$ *vs*. the **a2** treated samples (F and G).

inhibition rate in MGC-803 cells with reduced expression of SLC7A11 (Fig. S4C and S4D), suggesting that decreasing of SLC7A11 enhanced the response of cells to **a2**. We also examined the expression level of SLC7A11, and found no observed relationship between SLC7A11 protein level and GI_{50} values of **a2** (Fig. S4A and Fig. 1B). Together, these data supported that **a2** inhibited cell growth by decreasing GPX4 expression, while elevated SLC7A11 antagonized anti-proliferative activity of **a2**.

3.5. *Compound **a2** induced cell ferroptosis by causing ferrous iron (Fe^{2+}) accumulation*

Given that ferroptosis is a form of regulated cell death driven by iron-dependent lipid peroxidation, we tested the ferrous iron content in the presence of **a2**. As shown in Fig. 5A, **a2** significantly increased ferrous iron accumulation in both MGC-803 and MKN-45 cells. In accordance with that, iron chelater deferoxamine can markedly reverse the cell growth prevented by **a2** in gastric cancer cells (Fig. 5B and C). Considering that autophagy can cause excessive extracellular iron by degrading the iron storage protein ferritin, an inhibitor of autophagy 3-MA was utilized to explore the function of autophagy in **a2**-induced ferrous iron accumulation[24,25]. As expected, ferrous iron accumulation triggered by **a2** could be completely prevented by 3-MA in both MGC-803 and MKN-45 cells, indicating that **a2** induced an excess of ferrous iron through autophagy (Fig. 5D and E). Consistent with this, **a2** can dose-dependently induce the expression of LC3B (Supporting Information Fig. S5), and the relative inhibitory rate induced by the combination of **a2** and 3-MA was significantly lower than that of **a2** alone (Fig. 5F and G). Taken together, **a2**

induced cell growth inhibition through autophagy-dependent ferrous iron accumulation.

*3.6. Compound **a2** inhibited tumor growth in both the CDX and PDX models of gastric cancer, and downregulation of GPX4 indicated the sensitivity of PDX models to **a2***

Based on the fact that **a2** markedly inhibited the growth of gastric cancer cells, we further measured the anti-tumor efficacy of **a2** in MGC-803 CDX mice models. As shown in Fig. 6A and B and Supporting Information Fig. S6A, **a2** dose- and time-dependently inhibited tumor growth; the anti-tumor efficacy of **a2** at 10 or 20 mg/kg were more potent than that of the positive control drug 5-FU. In addition, **a2** had fewer effect on mouse body weight compared to 5-FU (Fig. S6B). We also performed pathologic examination of the main organs and hematology test to evaluate the adverse effects of **a2** in mice. Compared with the saline group, groups with **a2** and 5-FU showed no observed adverse effects on the heart, liver, spleen, lung, and kidney (Fig. S6C). Furthermore, **a2** and 5-FU had minor effects on the number of white blood cells, red blood cells, hemoglobin and platelets compared to the saline (Fig. S6D). Thus, **a2** exhibited strong anti-tumor efficacy with minor adverse effects in CDX mice models of gastric cancer.

As **a2** inhibited tumor growth with minor adverse effects, we next measured the anti-tumor activity of **a2** in gastric cancer PDX models. As shown in Fig. 6C, **a2** inhibited tumor growth with a range of tumor growth inhibition T/C ratios from 19.9% to 129.1%, indicating that the tumors in PDX models displayed diverse sensitivity to **a2**. The respective tumor volume and time curve of **a2** in different gastric cancer PDX mice models were supplied in Supporting Information Fig. S7. We further measured the expression of GPX4 at the end of treatment, and found that **a2** decreased expression of GPX4 in sensitive PDX models including PDX-01, PDX-02, and PDX-03, whereas GPX4 displayed resistant to **a2** in resistant PDX models, which was in consistent with previous data that **a2** induced ferroptosis by downregulating GPX4 (Fig. 6D). In contrast, the anti-tumor activity of 5-FU in PDX models showed no relationship with GPX4 expression. Therefore, these results indicated that **a2** differentially inhibited tumor growth in PDX models and that downregulation of GPX4 can be a biomarker to indicate the sensitivity of **a2** against tumors.

*3.7. Compound **a2** exhibited good pharmacokinetic characteristics*

The excellent anti-tumor activity of **a2** encouraged us to evaluate its pharmacokinetic parameters. The Caco-2 cell permeability assay was used to measure the human intestinal absorption of **a2**. As shown in Table 1, the apparent permeability coefficient (P_{app}) value of propranolol was 28.31, which was a highly membrane permeable compound. The P_{app} (A–B) values of atenolol and digoxin, which are poorly permeable agents, were both less than 1. The P_{app} (A–B) value of tested **a2** was 16.08, which is between 28.31 and 0.13, suggesting that **a2** was a moderately permeable compound against the Caco-2 monolayer from A to B. P_{app}

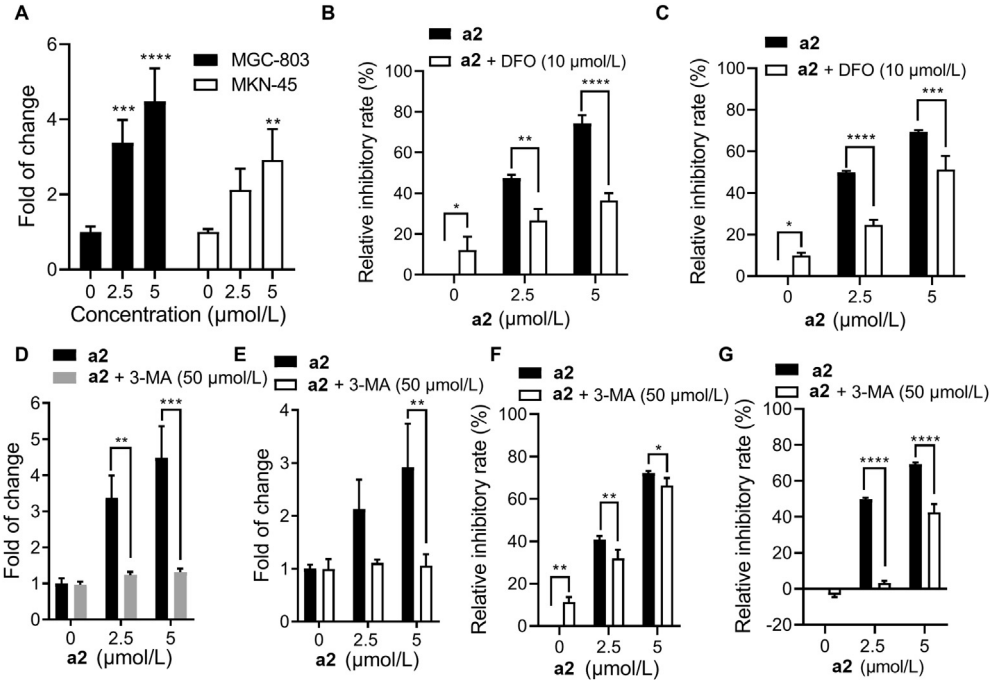

Figure 5 Compound **a2** induced ferroptosis through accumulation of ferrous iron. (A) Ferrous iron contents were measured in MGC-803 and MKN-45 cells treated with **a2** for 24 h. Relative inhibitory effects of **a2** without or with deferoxamine on MGC-803 (B) and MKN-45 (C) cells (72 h). MGC-803 (D) and MKN-45 (E) cells were treated with **a2** alone or combined with 3-MA for 24 h, ferrous iron contents were then examined. MGC-803 (F) and MKN-45 (G) cells were treated with indicated compounds for 72 h, relative inhibitory rates were tested. Data are presented as the mean ± SD ($n = 3$) from three independent experiments with biological duplicates in (A−G). Statistics differences were analyzed by two-way ANOVA analysis: $^{**}P < 0.05$, $^{***}P < 0.005$, $^{****}P < 0.001$ *vs*. the control (A). $^{*}P < 0.05$, $^{**}P < 0.01$, $^{***}P < 0.005$, $^{****}P < 0.001$ *vs*. the **a2** treated samples (B−G).

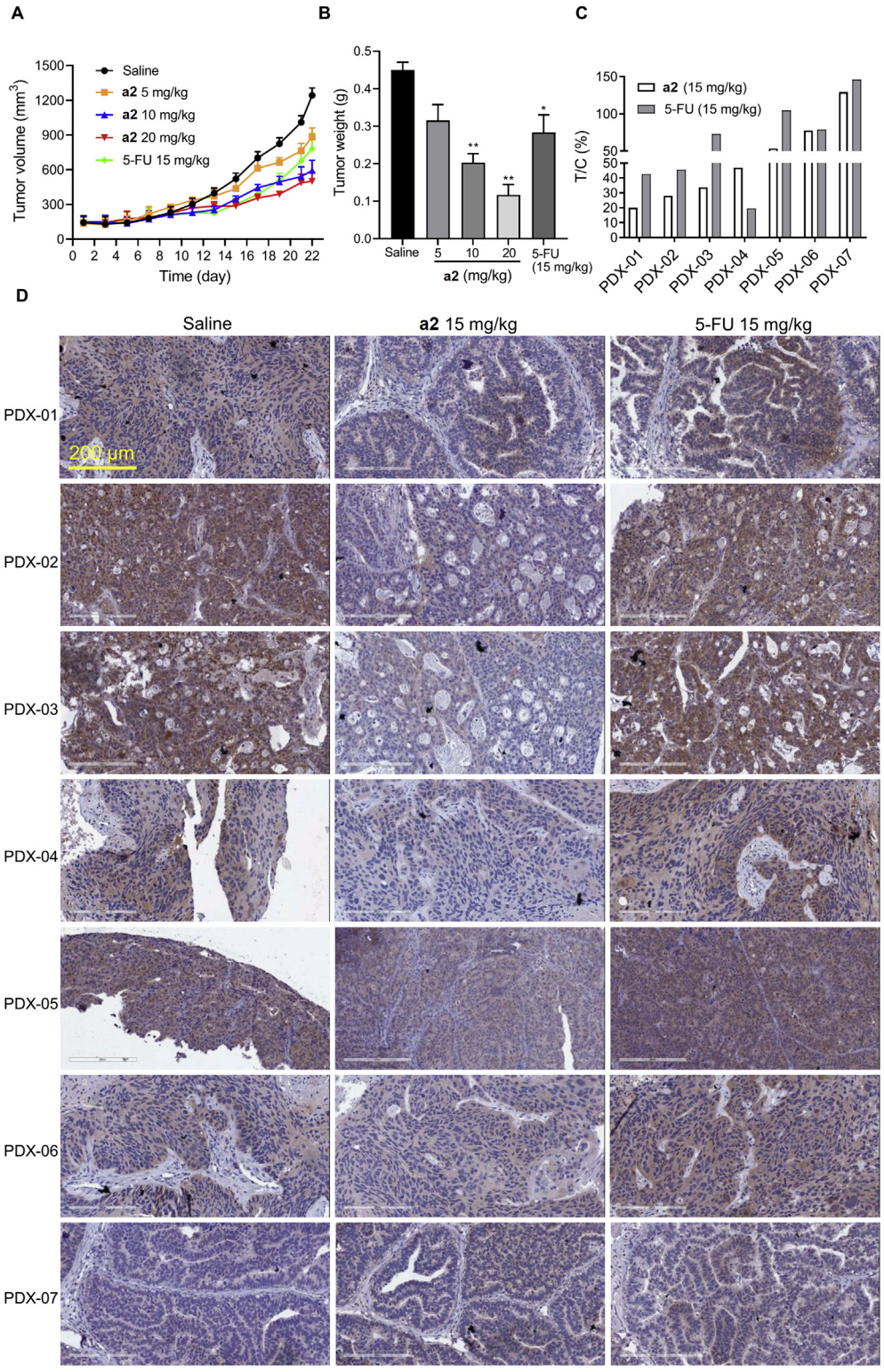

Figure 6 Compound **a2** inhibited tumor growth in both CDX and PDX models of gastric cancer. (A) Male mice bearing MGC-803 xenograft were treated with indicated agents once a day for 21 days, tumor volume was measured periodically. Data are presented as the mean ± SD ($n = 6$). (B) Average tumor weights with indicated agents at the end of treatment. Data are presented as the mean ± SD ($n = 6$). Statistics differences were analyzed by one-way ANOVA analysis: $^{*}P < 0.05$, $^{**}P < 0.01$ *vs*. the saline group. (C) Tumor growth inhibition T/C ratio of indicated compounds were measured at the end of treatment in mice bearing specific gastric cancer patient derived xenografts. (D) Expression of GPX4 in tumor tissues from PDX modes was determined by IHC.

(B–A)/P_{app} (A–B) is also called the efflux ratio and can quantify the levels of active efflux. A compound with an efflux ratio greater than 2 is subject to active efflux. The efflux ratios of atenolol and digoxin were 9.8 and 196.6, respectively, which represented active efflux. The P_{app} (B–A)/P_{app} (A–B) value of **a2** was 0.2, suggesting that **a2** will not undergo active efflux.

Metabolic stability plays an important role in substance clearance, thus we used liver microsomes from human, rat, mouse, dog and monkey to measure the *in vitro* intrinsic clearance of **a2**. As shown in Fig. 7A and Table 2, the concentration–time curve of the positive control substance, verapamil, varied among different species according to the duration of metabolism, suggesting that $Cl_{human} < Cl_{dog} < Cl_{rat} < Cl_{mouse} < Cl_{monkey}$. Compared with verapamil, **a2** displayed an undifferentiated efficacy of metabolism in different species, with $t_{1/2}$ values ranging from 23.5 to 34.9 min. Thus, **a2** exhibited strong microsomal metabolic stability with minor species diversity.

We further evaluated the pharmacokinetic (PK) parameters of **a2** in male SD rats, the mean plasma concentration–time curve and corresponding PK parameters of **a2** were shown in Fig. 7B and Table 3. The C_{max} value of **a2** was 18,319 ng/mL. The half-life and mean residence time were 3.93 and 1.54 h, respectively. According to a previous report, the $t_{1/2}$ value of 5-FU upon intraperitoneal injection in mice is 1.36 h, which is shorter than that of **a2**[26]. Therefore, these data indicated that **a2** had superior pharmacokinetic characteristics.

4. Discussion

JDA was first isolated and identified from Jiyuan *R. rubescens* early in 2011 by our group, after which several JDA analogues showed anti-tumor activity against esophageal and gastric cancer cells[3,27,28]. However, poorly known mechanism of action and bioavailability hinder the clinical development of compound JDA. In this study, we found a novel JDA derivative, **a2**, selectively inhibited the proliferation of gastric cancer cells. Induction of ferroptosis by downregulating GPX4 and ferrous iron accumulation mainly contributed to the anti-tumor activity of **a2** in gastric cancer cells. Results from the CDX and PDX models of gastric cancer further confirmed the anti-tumor efficacy of **a2**, and the downregulation of GPX4 predicted the sensitivity of tumors to **a**2 in gastric cancer PDX models. Importantly, **a2** exhibited superior PK characteristics. Therefore, the excellent anti-tumor activity and PK characteristics of **a2** make it a promising anti-tumor agent for gastric cancer treatment.

Our results indicated that **a2** inhibited cell cycle at the G2/M phase, which was in accordance with previous reports that JDA analogues (jaridonin and JDA-202) induce the G2/M arrest in esophageal cancer cells[8,27]. We also observed that **a2** caused mitochondria-dependent apoptosis in gastric cancer cells. However, prevention of apoptosis only partially antagonized the anti-proliferative activity of **a2** only in MGC-803 cells and not in MKN-45 cells. These results suggested that **a2** may inhibit cell growth through different mechanisms in different gastric cancer cell lines. And apoptosis may be an alternative or secondary event caused by **a2** and contributed little to the anti-proliferative activity of **a2**.

Ferroptosis is a recently discovered form of programmed cell death executed by the interaction of ROS and ferrous iron, resulting in lipid ROS burst and cell death[14,29]. RNA-seq analysis of MGC-803 cells treated with **a2** indicated that significantly differentiated mRNAs enriched in ferroptosis, lipid peroxidation

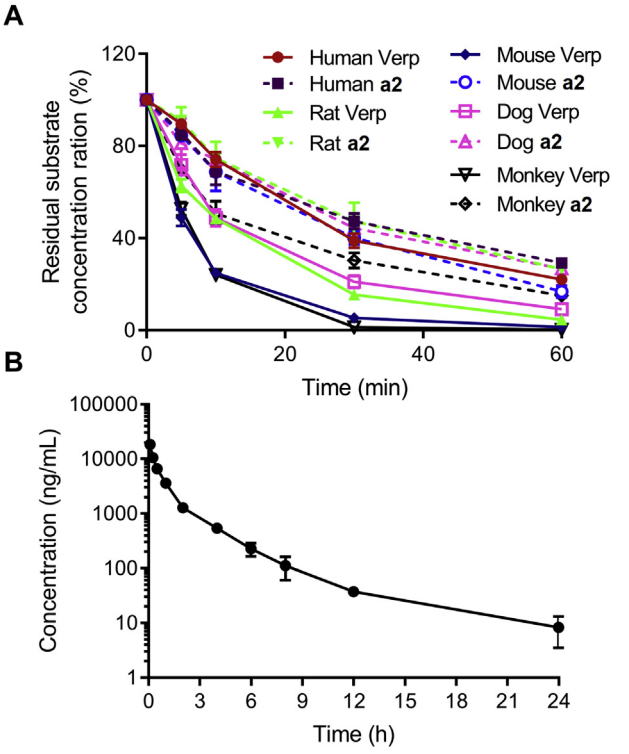

Figure 7 Pharmacokinetic characteristics of compound **a2**. (A) Microsomal metabolic stability of **a2** (1 μmol/L) in liver microsomes from indicated species. Verapamil (Verp) was selected as a positive control. Data are presented as the mean ± SD (n = 2). (B) Mean plasma concentration–time profile of **a2** after an intravenous administration of **a2** (20 mg/kg) to male SD rats. Data are presented as the mean ± SD (n = 3).

Table 1 Permeability coefficients of the compounds **a2**.

Test sample	Direction	P_{app} (10^{-6} cm/s) Mean ± RSD	P_{app} (B–A)/P_{app} (A–B)
Propranolol	A–B	28.31 ± 0.43	0.7
	B–A	18.5 ± 0.3	
Atenolol	A–B	0.23 ± 0.02	9.8
	B–A	2.2 ± 0.1	
Digoxin	A–B	0.13 ± 0.02	196.6
	B–A	24.7 ± 0.1	
a2	A–B	16.08 ± 1.01	0.2
	B–A	3.3 ± 0.3	

Table 2 The $t_{1/2}$ of compound **a2** and verapamil in liver microsomes of different species.

Species	$t_{1/2}$ (min)		CL (μL/min/mg)	
	a2	Verapamil	**a2**	Verapamil
Human	34.9	26.9	99.4	128.8
Rat	31.2	13.7	111.2	252.7
Mouse	23.7	10	146.3	347.3
Dog	32.2	17.8	107.7	194.8
Monkey	23.5	4.8	147.7	725.7

Table 3 Main pharmacokinetic parameters of **a2** in rats.

PK parameter	**a2**
C_{max} (ng/mL)	18319.0 ± 1422.0
$t_{1/2}$ (h)	3.93 ± 0.48
AUC_{last} (h·ng/mL)	14804.9 ± 1322.1
AUC_{INF_pred} (h·ng/mL)	14840.8 ± 1328.4
CL_{pred} (L/h/kg)	1.65 ± 0.23
$V_{z\text{-}pred}$ (L/kg)	7.73 ± 1.46
MRT_{last} (h)	1.54 ± 0.13

assay and transmission electron microscope data confirmed that **a2** induced ferroptosis in both MGC-803 and MKN-45 cells. GPX4 is an enzyme that catalyzes the reduction of lipid peroxides and plays an essential role in regulation of ferroptosis, and inhibition of GPX4 is a promising strategy to treat refractory cancer[30,31]. Compound **a2** downregulated expression of GPX4 and overexpression of GPX4 markedly attenuated the anti-proliferative activity of **a2** in both MGC-803 and MKN-45 cells, suggesting that downregulation of GPX4 played a critical role in **a2**-induced cell growth inhibition. Consistent with this, the expression of GPX4 was only inhibited by **a2** in sensitive gastric cancer PDX models, making GPX4 downregulation a promising biomarker. We also found that **a2** upregulated SLC7A11 and inhibiting SLC7A11 with specific SLC7A11 inhibitor or specific siRNAs enhanced the anti-proliferative activity of **a2**. It has been reported that JDA analogues jaridonin and JDA-202 cause upregulation of P53, and P53 can inhibit ferroptosis by repression of the SLC7A11[8,27,32]. In contrast, **a2** had no effect on the mRNA and protein levels of P53 in MGC-803 cells (data not shown), suggesting that **a2** exerted anti-tumor activity with new mechanism.

Compound **a2** caused accumulation of ferrous iron, which interacts with ROS to produce large amounts of lipid ROS. Iron homeostasis plays an essential role in cell survival and is well regulated by multiple pathways[33]. Inhibition of autophagy antagonized ferrous iron accumulation and cell growth inhibition caused by **a2**, which was in accordance with previous report that *ent*-kaurane diterpenoid oridonin induces autophagy in P53-mutated colorectal cancer cells[34].

5. Conclusions

Taken together, we found a novel JDA derivative, **a2**, which showed excellent anti-tumor efficacy with minor adverse effects in both gastric cancer cells and mouse models. Compound **a2** selectively inhibited tumor growth in gastric cancer PDX models that in which GPX4 expression can be suppressed. It is well known that gastric cancer a kind of cancers with highly heterogeneity with diverse molecular features. Downregulation of GPX4 can thus be a biomarker to indicate the anti-tumor activity of **a2** in gastric cancer.

Acknowledgments

This work was supported by grants from the National Natural Science Foundation of China (Nos. 81773562, 82020108030, and U1904163), National Key Research and Development Project (No. 2018YFE0195100, China), and the Science and Technology Program of Henan Province (No. 202102310152, China).

Author contributions

Yichao Xu, Dequan Yu, Hongmin Liu conceived and designed all the experiments and revised the manuscript. Ying Liu conducted the majority experiments, analyzed data and wrote original draft. Zan Song conducted the animal assays. Yajie Liu and Xubin Ma carried out the ROS determination and ferrous iron assay. Wang Wang and Yu Ke isolated JDA and synthesized compound **a2**.

Conflicts of interest

The authors declare no conflicts of interest.

Appendix A. Supporting information

Supporting data to this article can be found online at https://doi.org/10.1016/j.apsb.2021.05.006.

References

1. Bray F, Ferlay J, Soerjomataram I, Siegel RL, Torre LA, Jemal A. Global cancer statistics 2018: GLOBOCAN estimates of incidence and mortality worldwide for 36 cancers in 185 countries. *CA Cancer J Clin* 2018;**68**:394–424.
2. Smyth EC, Nilsson M, Grabsch HI, van Grieken NC, Lordick F. Gastric cancer. *Lancet* 2020;**396**:635–48.
3. Liu HM, Zhu CG, Wang QD, Ke Y, Liu ZZ, Yan XB, et al., inventors. Novel *ent*-kaurene diterpene compound and its derivatives, their preparation and their use. US patent US8084430B2. 2011 Dec 27.
4. Zhang Y, Wang S, Dai M, Nai J, Zhu L, Sheng H. Solubility and bioavailability enhancement of oridonin: a review. *Molecules* 2020;**25**:332–55.
5. Sarwar MS, Xia YX, Liang ZM, Tsang SW, Zhang HJ. Mechanistic pathways and molecular targets of plant-derived anticancer *ent*-kaurane diterpenes. *Biomolecules* 2020;**10**:144–61.
6. Wang JN, Zhang ZR, Che Y, Yuan ZY, Lu ZL, Li Y, et al. Acetylmacrocalin B, an *ent*-kaurane diterpenoid, initiates apoptosis through the ROS-p38-caspase 9-dependent pathway and induces G2/M phase arrest *via* the Chk1/2-Cdc25C-Cdc2/cyclin B axis in non-small cell lung cancer. *Cancer Biol Ther* 2018;**19**:609–21.
7. Li Y, Li N, Shi J, Ahmed T, Liu H, Guo J, et al. Involvement of glutathione depletion in selective cytotoxicity of oridonin to p53-mutant esophageal squamous carcinoma cells. *Front Oncol* 2019;**9**:1525–35.
8. Shi XJ, Ding L, Zhou W, Ji Y, Wang J, Wang H, et al. Pro-apoptotic effects of JDA-202, a novel natural diterpenoid, on esophageal cancer through targeting peroxiredoxin I. *Antioxidants Redox Signal* 2017;**27**:73–92.
9. Huang H, Weng H, Dong B, Zhao P, Zhou H, Qu L. Oridonin triggers chaperon-mediated proteasomal degradation of BCR-ABL in leukemia. *Sci Rep* 2017;**7**:41525–37.
10. He HB, Jiang H, Chen Y, Ye J, Wang AL, Wang C, et al. Oridonin is a covalent NLRP3 inhibitor with strong anti-inflammasome activity. *Nat Commun* 2018;**9**:2550–6.
11. Song M, Liu X, Liu K, Zhao R, Huang H, Shi Y, et al. Targeting AKT with oridonin inhibits growth of esophageal squamous cell carcinoma *in vitro* and patient-derived xenografts *in vivo*. *Mol Cancer Therapeut* 2018;**17**:1540–53.
12. Su Y, Zhao B, Zhou L, Zhang Z, Shen Y, Lv H, et al. Ferroptosis, a novel pharmacological mechanism of anti-cancer drugs. *Cancer Lett* 2020;**483**:127–36.
13. Koppula P, Zhuang L, Gan B. Cystine transporter SLC7A11/xCT in cancer: ferroptosis, nutrient dependency, and cancer therapy. *Protein Cell* 2020. Available from: https://doi.org/10.1007/s13238-020-00789-5.

14. Battaglia AM, Chirillo R, Aversa I, Sacco A, Costanzo F, Biamonte F. Ferroptosis and cancer: mitochondria meet the "iron maiden" cell death. *Cells* 2020;**9**:1505−31.
15. Hassannia B, Vandenabeele P, Vanden Berghe T. Targeting ferroptosis to iron out cancer. *Cancer Cell* 2019;**35**:830−49.
16. Wang J, Yin X, He W, Xue W, Zhang J, Huang Y. SUV39H1 deficiency suppresses clear cell renal cell carcinoma growth by inducing ferroptosis. *Acta Pharm Sin B* 2021;**11**:406−19.
17. Li LM, Li GY, Ding LS, Yang LB, Zhao Y, Pu JX, et al. *ent*-Kaurane diterpenoids from isodon nervosus. *J Nat Prod* 2008;**71**:684−8.
18. Wang S, Ma XB, Yuan XH, Yu B, Xu YC, Liu HM. Discovery of new [1,2,4]triazolo[1,5-*a*]pyrimidine derivatives that kill gastric cancer cells *via* the mitochondria pathway. *Eur J Med Chem* 2020;**203**:112630−42.
19. Love MI, Huber W, Anders S. Moderated estimation of fold change and dispersion for RNA-seq data with DESeq2. *Genome Biol* 2014;**15**:550−71.
20. Yu GC, Wang LG, Han YY, He QY. clusterProfiler: an R package for comparing biological themes among gene clusters. *OMICS* 2012;**16**:284−7.
21. Sun PY, Wu GL, Qiu ZJ, Chen YJ, inventors. L-Alanine-(14-oridonin) ester trifluoroacetate as well as preparation method and application. Chinese patent CN104017000B. 2017 Jan 04.
22. Green DR, Llambi F. Cell death signaling. *Cold Spring Harb Perspect Biol* 2015;**7**:a006080.
23. Stockwell BR, Friedmann Angeli JP, Bayir H, Bush AI, Conrad M, Dixon SJ, et al. Ferroptosis: a regulated cell death nexus linking metabolism, redox biology, and disease. *Cell* 2017;**171**:273−85.
24. Liu J, Kuang F, Kroemer G, Klionsky DJ, Kang R, Tang D. Autophagy-dependent ferroptosis: machinery and regulation. *Cell Chem Biol* 2020;**27**:420−35.
25. Alu A, Han X, Ma X, Wu M, Wei Y, Wei X. The role of lysosome in regulated necrosis. *Acta Pharm Sin B* 2020;**10**:1880−903.
26. Smith T, Affram K, Nottingham EL, Han B, Amissah F, Krishnan S, et al. Application of smart solid lipid nanoparticles to enhance the efficacy of 5-fluorouracil in the treatment of colorectal cancer. *Sci Rep* 2020;**10**:16989−7003.
27. Ma YC, Ke Y, Zi X, Zhao W, Shi XJ, Liu HM. Jaridonin, a novel *ent*-kaurene diterpenoid from Isodon rubescens, inducing apoptosis *via* production of reactive oxygen species in esophageal cancer cells. *Curr Cancer Drug Targets* 2013;**13**:611−24.
28. Ma YC, Su N, Shi XJ, Zhao W, Ke Y, Zi X, et al. Jaridonin-induced G2/M phase arrest in human esophageal cancer cells is caused by reactive oxygen species-dependent Cdc2-tyr15 phosphorylation *via* ATM-Chk1/2-Cdc25C pathway. *Toxicol Appl Pharmacol* 2015;**282**:227−36.
29. Dixon SJ, Lemberg KM, Lamprecht MR, Skouta R, Zaitsev EM, Gleason CE, et al. Ferroptosis: an iron-dependent form of non-apoptotic cell death. *Cell* 2012;**149**:1060−72.
30. Yang WS, SriRamaratnam R, Welsch ME, Shimada K, Skouta R, Viswanathan VS, et al. Regulation of ferroptotic cancer cell death by GPX4. *Cell* 2014;**156**:317−31.
31. Hangauer MJ, Viswanathan VS, Ryan MJ, Bole D, Eaton JK, Matov A, et al. Drug-tolerant persister cancer cells are vulnerable to GPX4 inhibition. *Nature* 2017;**551**:247−50.
32. Jiang L, Hickman JH, Wang SJ, Gu W. Dynamic roles of p53-mediated metabolic activities in ROS-induced stress responses. *Cell Cycle* 2015;**14**:2881−5.
33. Bogdan AR, Miyazawa M, Hashimoto K, Tsuji Y. Regulators of iron homeostasis: new players in metabolism, cell death, and disease. *Trends Biochem Sci* 2016;**41**:274−86.
34. Yao Z, Xie F, Li M, Liang Z, Xu W, Yang J, et al. Oridonin induces autophagy *via* inhibition of glucose metabolism in p53-mutated colorectal cancer cells. *Cell Death Dis* 2017;**8**:e2633.